

Imaging superatomic molecular orbitals in a C_{60} molecule through four 800-nm photons

G. P. Zhang,^{1,*} H. P. Zhu,^{1,2} Y. H. Bai³, J. Bonacum¹, X. S. Wu², and Thomas F. George⁴

¹*Department of Physics, Indiana State University, Terre Haute, Indiana 47809, USA*

²*Laboratory of Solid State Microstructures and School of Physics,
Nanjing University, Nanjing 210093, China*

³*Office of Information Technology, Indiana State University,
Terre Haute, Indiana 47809, USA and*

⁴*Office of the Chancellor and Center for Nanoscience
Departments of Chemistry & Biochemistry and Physics & Astronomy
University of Missouri-St. Louis, St. Louis, MO 63121, USA*

(Dated: November 2, 2021)

Abstract

Superatomic molecular orbitals (SAMO) in C_{60} are ideal building blocks for functional nanostructures. However, imaging them spatially in the gas phase has been unsuccessful. It is found experimentally that if C_{60} is excited by an 800-nm laser, the photoelectron casts an anisotropic velocity image, but the image becomes isotropic if excited at a 400-nm wavelength. This diffuse image difference has been attributed to electron thermal ionization, but more recent experiments (800 nm) reveal a clear non-diffuse image superimposed on the diffuse image, whose origin remains a mystery. Here we show that the non-diffuse anisotropic image is the precursor of the f SAMO. We predict that four 800-nm photons can directly access the $1f$ SAMO, and with one more photon, can image the orbital, with the photoelectron angular distribution having two maxima at 0° and 180° and two humps separated by 56.5° . Since two 400-nm photons only resonantly excite the spherical $1s$ SAMO and four 800-nm photon excite the anisotropic $1f$ SAMO, our finding gives a natural explanation of the non-diffuse image difference, complementing the thermal scenario.

PACS numbers: 79.20.Ws, 78.66.Tr, 42.30.-d, 78.40.-q

Keywords:

I. INTRODUCTION

In nanoscience, no other cluster has ever garnered more attention than C_{60} [1]. Such a highly symmetric molecule allows a high electron delocalization, enabling ultrafast dynamics [2, 3], strong nonlinear optical responses [4, 5], and high harmonic generation [6, 7]. Recently, employing scanning tunneling microscopy (STM), Feng *et al.* [8] discovered a group of unusually large orbitals both inside and outside of the C_{60} cage, which are both beautiful and surprising. These orbitals, called superatomic molecular orbitals (SAMOs), have attracted immediate attention [9, 10]. Spatially, they bear a close resemblance to their atomic counterparts, but with a much larger radius. This motivated Roy and coworkers [11] to design nanoscale atoms for solid-state chemistry. Figure 1 shows a $1f$ orbital, where one sees a distinctive anisotropy characteristic of f orbitals. However, imaging such high-lying orbitals becomes increasingly difficult for STM, because of the strong overlap between the orbitals of C_{60} and those of the substrates.

The velocity-map imaging technique [12, 13] does not have this problem, since it works in the gas phase. Figure 1 schematically shows that after the laser strikes C_{60} , the photoelectrons with different velocities, after several stages of accelerating electrode plates, cast an image on the phosphor screen, which is captured by the CCD camera. This image carries the orbital information. Doing so, quite surprisingly, neither Johansson *et al.* [10] nor Kjellberg *et al.* [14] detected any image similar to superorbitals. Instead, they reported a seemingly irrelevant observation: The electron image is anisotropic if excited by an 800-nm laser, but is isotropic with a 400-nm laser. How could it be possible that a similar observation in ion yields (ellipticity dependence) [15, 16] occurs for the electrons as well? Huisman *et al.* [17] further showed that the anisotropy increases with the laser intensity, and they assigned it to the accumulation of highly structured but slightly different angular distributions of the ground states, while others assign the diffuse part of the photoelectron spectrum to thermal electron ionization [14] or a “kick” from the laser field [10], with an explanation presented in the second paper of Ref. [10]. Huisman *et al.* emphasized that a fully satisfactory theory requires a complete *ab initio* calculation. Such a calculation is now available [18], but these studies did not address the difference between the 800-nm and 400-nm excitations. Very recently, Li and coworkers experimentally showed a distinct and non-diffuse image superimposed on the diffuse anisotropic background [19]. These non-diffuse features can not easily

be explained by the thermal electron ionization, since the Boltzmann-like distribution is unlikely to yield an image with intensities only concentrated at six spatial locations. We wonder how such nondiffuse images are formed, besides the origin in the thermal electron ionization.

In this paper, we demonstrate theoretically that SAMOs in C_{60} in general, and the $1f$ orbital in particular, are accessible to the velocity map imaging technique. Our first important prediction is that the energy gap between the $1f$ orbital and HOMO matches the four-photon energy of an 800-nm laser pulse. By successively absorbing four photons, electrons in the HOMO can be excited into the $1f$ orbital; by absorbing one extra photon, they are cleared of the ionization potential energy of 7.58 eV, and can then be detected by the velocity map imaging. We further predict that the angular resolved spectrum has a distinctive $1f$ orbital feature, with two local maxima, separated by 56.5° . There are two reasons why the $1f$ orbital can be effectively probed. First, the multiphoton excitation suppresses an otherwise strong contribution from nonSAMOs. Second, although energetically d and g SAMOS are in the vicinity of the $1f$ orbital, due to the selection rule, transitions to those orbitals are not possible. Such a detection scheme is quite generic. By slightly tuning the photon energy of the laser beam, it is also possible to observe $2p$, $3p$ and $1h$ orbitals. If C_{60} is excited by two 400-nm photons, the strongest transition is between HOMO-1 and nonSAMOs, but this transition is off-resonant by 0.62 eV. On the other hand, although the transition matrix element product is small for the transition from HOMO-2 to $1s$ SAMO, this transition is nearly resonant, and it is likely that the $1s$ SAMO is excited, consistent with Ref. [10]. Therefore, our study suggests a new and alternative explanation to the anisotropic and non-diffuse image [19], and demonstrates the new power of multiphoton emission for investigating SAMOs in fullerenes.

II. THEORETICAL FORMALISM

We employ two complementary first-principles methods within the density functional theory: the basis function-based methods (Gaussian09 [20] and VASP [21]) and the real grid mesh method (Octopus) [22]. To build a case to directly probe SAMOs in C_{60} , we first investigate the density functionals' effect on the energy gap between the HOMO and $1f$ SAMO for a group of six different functionals, within the same basis 6-311+G(d). Figure

2(a) shows that the functional has a substantial impact on the energy gap ΔE (see the filled red circles). Since the ionization potential (IP) is at 7.58 eV (the dashed green line) and 1*f* SAMO must be a few eV below IP, some popular functionals such as B3LYP and CAM-B3LYP predict the results too large even in the single-particle limit. This result is rigorous since it does not involve the complicated photoexcitation and ionization. This convinces us that the SWVN/LDA functional is reliable, at least within the single-particle limit.

Next, we employ the same SWVN/LDA functional but increase the basis function size by adding more diffuse functions [9] to the Gaussian basis. When we use the aug-cc-pvtz basis, we find that ΔE drops to 7.136 eV (see the empty red circle in Fig. 2(a)). We then put a layer of 60 fictitious hydrogen atoms at a radius of 9 Å from the center of C₆₀. These atoms have no charge and only serve as the centers for additional basis functions. The carbon atoms have the 6-311+G(d) basis, while those fictitious hydrogen atoms have aug-cc-pV6Z, which contains 7*s*, 6*p*, 5*d*, 4*f*, 3*g* and 2*h* Gaussian primitive functions. Doing so, we find that the LDA gap $\Delta E_{1f,LDA}$ decreases from 7.506 eV (without fictitious atoms) to 6.957 eV (with fictitious atoms), with the net change as large as 0.549 eV (compare the first two filled circles of Fig. 2(a)). It is convincing that the basis functions strongly affect the accuracy of the energy levels of SAMOs. However, if we continue to use the Gaussian primitives, the calculation becomes increasingly demanding. We must pursue a different approach.

To gradually eliminate the basis function effect, we employ a grid mesh-based method as implemented in Octopus [22]. An important advantage is that the real grid is a balanced approach and treats SAMOs and nonSAMOs on an equal footing. Figure 2(a) shows that as r increases (the bottom horizontal axis represents r), ΔE gradually converges to 6.337 eV (see the squares at the bottom of the figure). We then fit the data to $\Delta E = \Delta E_0 + \Delta E_1/r$ and find $\Delta E_0 = 6.015$ eV and $\Delta E_1 = 10.0707$ eV/Å. $\Delta E_0 = 6.015$ eV is considered as a lower limit for this gap. As an independent check, we employ a planewave basis function as implemented in the VASP code [21], where we place C₆₀ in a big fcc supercell with two respective lattice constants of $a = 21$ Å and 25 Å, and two planewave cutoffs of 500 and 600 eV. The results are shown in Fig. 2(a) (see the plus signs). The VASP result is 6.36 eV, which is considered as an upper limit. If we average these two limits, we expect that this gap settles down at 6.2 eV, which precisely matches the four-photon energy of a laser pulse of wavelength 800 nm. Figure 2(b) shows the energy spectrum of SAMOs referenced to the HOMO. For an 800-nm laser, five photons are needed to reach the IP (see the thick dashed

green line on the top). The fourth photon has access to the SAMOs which are congested in a narrow window. Figure 2(c) zooms in on the SAMOs. Consistent with Feng’s VASP result [8], the gap between the s SAMO and LUMO is 3.25 eV, but our interest is in higher SAMOs. This energy gap becomes an outstanding case to judge the quality of the two most popular density functionals, LDA versus B3LYP. If the LDA result is correct, then an 800-nm laser can detect $1f$ SAMO experimentally. This is the first testable case for experiments.

III. TWO-PHOTON VERSUS FOUR-PHOTON EXCITATION

Regardless of the experimental finding, such a multiphoton excitation requires a stronger laser. Would it be possible to do the same job with two UV photons as Johansson *et al.* [18] did? In order to have a successive optical transition from the occupied states to unoccupied states, the accumulative product of matrix elements of each transition must be different from zero. Different from prior studies, we compute the transition matrix elements between the HOMOs, SAMOs and nonSAMOs by integrating

$$\langle i|\mathbf{D}|j\rangle = \int_{-\infty}^{\infty} d\tau \psi_i(\mathbf{r})\mathbf{r}\psi_f(\mathbf{r}), \quad (1)$$

where $\psi_i(\mathbf{r})$ is the Kohn-Sham wavefunction, and \mathbf{r} is the electron coordinate. For the frequency-doubled case [18], at least two photons are needed to reach the $1f$ SAMO. Thus, we compute the product of two transition matrix elements, $\langle occ|\mathbf{D}|i\rangle\langle i|\mathbf{D}|j\rangle$, for all the relevant transitions around this two-photon energy. The results are surprising. Although there are lots of states energetically accessible, only a very few actually contribute. Figure 3(a) shows that for two-400-nm-photon photoexcitation, two groups of nonSAMOs have the largest product of the transition matrix elements, followed by f , s , d , g and h SAMOs. Although the nonSAMOs dominate the product of the matrix elements, their energies are off-resonant from two-400 nm photoexcitation. Specifically, the energy for two 400-nm photons is 6.2 eV, but the excitation from HOMO-1 to the nonSAMOs is 6.83 eV, off by 0.63 eV, which greatly reduces the excitation probability into the nonSAMOs. But for the $1s$ SAMO, although its matrix product is small, the excitation energy from HOMO-2 to $1s$ SAMO is 6.17 eV, nearly resonant with the two-400 nm photon energy of 6.2 eV. Therefore, during 400-nm excitation, the $1s$ SAMO is excited strongly. This finding is also consistent with Johansson’s assignment of their first peak to $1s$ SAMO [18]. Since the $1s$ SAMO is spherical, this explains why at

400-nm excitation the photoelectron image is isotropic, besides the contribution due to the diffuse mechanism as discussed above.

In the same spirit, we investigate the four-photon process. Four-photon excitations build upon four successive transitions, with the product of four transition moments as $\langle i|\mathbf{D}|j\rangle\langle j|\mathbf{D}|k\rangle\langle k|\mathbf{D}|l\rangle\langle l|\mathbf{D}|m\rangle$, where $|i\rangle$ is the HOMO, $|m\rangle$ are the SAMOs, and the others are intermediate states. Figure 3(b) plots the products for all the states with large contributions. Our results are insightful. First, the transition matrix element strictly obeys the dipole selection rule and has the correct parity. We see that only SAMOs with odd angular momentum quantum numbers have nonzero products. For instance, s and d SAMOs have no transition. Second, the SAMO dominates the four-photon transitions. The largest product is from the $1h$ SAMO, and the second largest is from the $1f$ SAMO, followed by the $2p$ and $3p$ SAMOs. It is likely that they compete with the $1f$ SAMO, but which one dominates depends sensitively on the actual photon energy, a finding that allows one to probe various SAMOs by tuning the laser wavelength. We also notice that the nonSAMO contribution is still sizable. Therefore, to observe SAMOs, future experiments must steer the laser wavelength away from those nonSAMOs energetically and use an optimal laser intensity (a laser too strong would populate other nonSAMOs). For an 800-nm laser, $1f$ is strongly excited, both in terms of the transition matrix elements and the transition energy. Since its shape is highly anisotropic (see the far right schematic in Fig. 1), this explains why experimentally Li and coworkers [19] find that the photoelectron image is non-diffusive and anisotropic, and more importantly has fine structures superimposed on the diffuse image seen before [10, 14]. To test our results quantitatively, we compute the kinetic energy of the electron. To eject this electron from $1f$ SAMO, one more photon is needed to clear the ionization potential energy $\text{IP} = 7.58$ eV. This leaves the ionized electron with a kinetic energy of $5h\nu - \text{IP} = 0.2$ eV. Sure enough, Fig. 2(e) of Ref. [18] indeed shows a peak at 0.2 eV, but this important finding did not catch the attention of the investigators, as their emphasis was on the 400-nm results.

IV. DISCUSSION

To really image the $1f$ orbitals, we have to overcome two challenges. First, since the $1f$ SAMO is seven-fold degenerate, would the final image of $1f$ SAMO be completely washed

out because of the spatial average during the experiment, in particular as C_{60} spins rather rapidly? This is an issue for the fluorescence spectrum in CO_2 , where the molecule has no preferred orientation. It has to be properly aligned before it can be imaged [23]. Fortunately, we find that the transition paths for seven $1f$ SAMOs are different, so their products of transition matrix elements are not the same. Thus, no spatial average is necessary. Numerically we find that they range from 3.2 to 2.1 \AA^4 (see the circles at the f SAMO in Fig. 3(b)). To understand the reason behind this, as an example, we take two $1f$ orbitals with spherical harmonics Y_{30} and Y_{31} , respectively. If the light is linearly polarized, for Y_{30} , the transition path can be like $|\text{HOMO}\rangle \rightarrow Y_{00} \rightarrow Y_{10} \rightarrow Y_{20} \rightarrow Y_{30}$, but for Y_{31} , $|\text{HOMO}\rangle \rightarrow |i\rangle \rightarrow |j\rangle \rightarrow Y_{11} \rightarrow Y_{21} \rightarrow Y_{31}$, where $|i(j)\rangle$ are two different intermediate states. Therefore, the experimental geometry (Fig. 1) intrinsically differentiates among different $1f$ states, already found in atoms [24]. In C_{60} we find that the dominant path or doorway state [25] is $|\text{HOMO}\rangle \rightarrow |1d\rangle \rightarrow |2p\rangle \rightarrow |2d\rangle \rightarrow |1f\rangle$.

The second challenge is whether $1f$ SAMO can ever cast its distinctive image on the final continuum state. We decide to compute the angular distribution of the electron density for an f orbital with the spherical harmonic Y_{30} . The intensity is proportional to the square of

$$\langle \psi(\vec{r}) | \vec{p} | e^{i\vec{k}\cdot\vec{r}} \rangle = 4\pi i^3 \hbar \vec{k} Y_{30}^*(\theta_k, \phi_k) \int_0^\infty dr R_f(r) j_3(kr) r^2, \quad (2)$$

where θ_k and ϕ_k define the direction of the wavevector \vec{k} of the ejected electron, and a constant term due to the orthogonality is not included. The angular distribution comes from $Y_{30}^*(\theta_k, \phi_k)$. Employing the realistic wavefunction of $1f$ SAMO in C_{60} , we compute the angular distribution of the $1f$ SAMO. The results are shown in Fig. 3(c). The maxima are at 0° and 180° , along the positive and negative directions on the z -axis, respectively (see the f SAMO in Fig. 1). As the angle rotates away from the z -axis, the intensity drops. We believe that this produces the anisotropy seen in the experiment [19]. The $1f$ SAMO has two distinctive double humps, separated by 56.5° . The unpublished experimental photoelectron angular distribution by Li and coworkers [19] is shown in Fig. 3(d). The agreement between our theory and their experiment is remarkable, where the shape, peak and hump locations are identical. We draw two dashed lines to highlight the locations of two humps; and our estimated experimental angle separation between them is 54.4° , in quantitative agreement with our theory within the experimental error. Figure 4.6(f) of Ref. [19] looks more like our predicted $1f$ SAMO (see Fig. 1). This constitutes a strong experimental support for our

theory.

V. CONCLUSION

While much attention has been given to the diffuse spectrum in VMI, recent experimental evidence shows a significant contribution from the non-diffuse photoelectrons [19]. Here we demonstrate through a series of carefully designed first-principles calculations that the non-diffuse and anisotropic velocity image observed at 800 nm is likely due to the excitation from the highest occupied molecular orbital into the $1f$ SAMO. We predict that the energy gap between the highest occupied molecular orbital and $1f$ SAMO matches the four-photon energy of 800 nm, and a peak at 0.2 eV will show up in the photoelectron spectrum. In agreement with the prior study, two 400-nm photons can excite $1s$ SAMO from HOMO-2 nearly resonantly, although nonSAMOs have a larger transition matrix product, but they are off resonance by 0.6 eV. Since the $1s$ SAMO is spherical, the photoelectron image is isotropic, in addition to the possible thermal and diffuse electron emission. Future experimental verification will have a series of important theoretical consequences. Which density functional, LDA or GGA, is more accurate to describe the photoelectron angular distribution and multiphoton emission? Which basis functions, Gaussian diffuse functions or real grid mesh, are more accurate to describe superorbitals? For the first time, we demonstrate that it is the multiphoton excitation that greatly boosts the transition probability into these superorbitals, a finding that is expected to inspire new experimental and theoretical investigations.

Acknowledgments

This work was supported by the U.S. Department of Energy under Contract No. DE-FG02-06ER46304 (GPZ). We acknowledge Hui Li, M. Kling, C. Lewis Cocke and Itzik Ben-Itzhak (Kansas State University) for making the data from Ref. [19] available to us. We also thank E. Glendenning (ISU) for the great help with the natural bond orbital analysis in Gaussian09, S. W. Robey (NIST) for sending us the Gaussian input file regarding Ref. [9], H. Petek (University of Pittsburgh) for their original paper [8], technical support from the Gaussian team on the pseudoatom applications, and D. Strubbe (MIT) for

helpful communications with Octopus. HPZ and XSW were supported by the National Natural Science Foundation of China (Contract Nos. 11274153, 10974081 and 10979017) and National Key Projects for Basic Research of China (Contract No. 2010CB923404). HPZ acknowledges support from China Scholarship Council during her stay in the United States and thanks Indiana State University for the hospitality under the exchange program. Part of the work was done on Indiana State University's Quantum clusters and HPC clusters. This research used resources of the National Energy Research Scientific Computing Center, which is supported by the Office of Science of the U.S. Department of Energy under Contract No. DE-AC02-05CH11231. This work was performed, in part, at the Center for Integrated Nanotechnologies, an Office of Science User Facility operated for the U.S. Department of Energy (DOE) Office of Science by Los Alamos National Laboratory (Contract DE-AC52-06NA25396) and Sandia National Laboratories (Contract DE-AC04-94AL85000).

*gpzhang@indstate.edu

-
- [1] H. Kroto, J. R. Heath, S. C. O'Brien, R. F. Curl, and R. E. Smalley, *Nature* **318**, 162 (1985).
 - [2] S. L. Dexheimer, D. M. Mittleman, R. W. Schoenlein, W. Vareka, X.-D. Xiang, A. Zettl, and C.V. Shank, in *Ultrafast Pulse Generation and Spectroscopy*, edited by T. R. Gosnell, A. J. Taylor, K. A. Nelson, and M.C. Downer, SPIE Proc. **1861**, 328 (1993); V. M. Farztdinov, A. L. Dobryakov, V. S. Letokhov, Yu. E. Lozovik, and Yu. A. Matveets, *Phys. Rev. B* **56**, 4176 (1997).
 - [3] G. P. Zhang and T. F. George, *Phys. Rev. B* **76**, 085410 (2007).
 - [4] Z. H. Kafafi, J. R. Lindle, R. G. S. Pong, F. J. Bartoli, L. J. Lingg, and J. Milliken, *Chem. Phys. Lett.* **188**, 492 (1992).
 - [5] G. P. Zhang and T. F. George, *Phys. Rev. Lett.* **109**, 257401 (2012).
 - [6] G. P. Zhang, *Phys. Rev. Lett.* **95**, 047401 (2005); G. P. Zhang and T. F. George, *Phys. Rev. B* **76**, 085410 (2007).
 - [7] R. A. Ganeev *et al.*, *Phys. Rev. Lett.* **102**, 013903 (2009).
 - [8] M. Feng, J. Zhao and H. Petek, *Science* **320**, 359 (2008); M. Feng, Y. Shi, C. Lin, J. Zhao, F. Liu, S. Yang, and H. Petek, *Phys. Rev. B* **88**, 075417 (2013); M. Feng, J. Zhao, T. Huang, X. Zhu, and H. Petek, *Acc. Chem. Res.* **44**, 360 (2011); J. Zhao, M. Feng, J. Yang, and H.

- Petek, ACS Nano **3**, 853 (2009).
- [9] G. J. Dutton, D. B. Dougherty, W. Jin, J. E. Reutt-Robey, and S. W. Robey, Phys. Rev. B **84**, 195435 (2011).
- [10] J. O. Johansson, J. Fedor, M. Goto, M. Kjellberg, J. Stenfalk, G. G. Henderson, E. E. B. Campbell, and K. Hansen, J. Chem. Phys. **136**, 164301 (2012); J. O. Johansson and E. E. B. Campbell, Chem. Soc. Rev. **42**, 5661 (2013); J. O. Johansson, E. Bohl, G. G. Henderson, B. Mignolet, T. J. S. Dennis, F. Remacle, and E. E. B. Campbell, J. Chem. Phys. **139**, 084309 (2013).
- [11] X. Roy *et al.*, Science **341**, 157 (2013).
- [12] A. T. J. B. Eppink and D. H. Parker, Rev. Sci. Instrum. **68**, 3477 (1997).
- [13] C. Bordas, F. Paulig, H. Helm, and D. L. Huestis, Rev. Sci. Instrum. **67**, 2257 (1996).
- [14] M. Kjellberg, O. Johansson, F. Jonsson, A. V. Bulgakov, C. Bordas, E. E. B. Campbell, and K. Jansen, Phys. Rev. A **81**, 023202 (2010).
- [15] I. V. Hertel *et al.*, Phys. Rev. Lett. **102**, 023003 (2009).
- [16] I. Shchatsinin, H.-H. Ritze, C. P. Schulz, and I. V. Hertel, Phys. Rev. A **79**, 053414 (2009).
- [17] Y. Huismans *et al.*, Phys. Rev. A **88**, 013201 (2013).
- [18] J. O. Johansson, G. G. Henderson, F. Remacle, and E. E. B. Campbell, Phys. Rev. Lett. **108**, 173401 (2012).
- [19] H. Li, *Study on molecular photoionization in femtosecond laser field*. Masters thesis (2013); unpublished but available at <http://jrm.phys.ksu.edu/theses.html>.
- [20] M. J. Frisch *et al.*, Gaussian09, Gaussian Inc. (Pittsburgh, PA, 2009).
- [21] G. Kresse and J. Furthmüller, Comput. Mater. Sci. **6**, 15 (1996).
- [22] X. Andrade, J. Alberdi-Rodriguez, D. A. Strubbe, M. J. T. Oliveira, F. Nogueira, A. Castro, J. Muguerza, A. Arruabarrena, S. G. Louie, A. Aspuru-Guzik, A. Rubio, and M. A. L. Marques, J. Phys.: Cond. Matt. **24**, 233202 (2012); A. Castro, H. Appel, M. Oliveira, C.A. Rozzi, X. Andrade, F. Lorenzen, M. A. L. Marques, E. K. U. Gross, and A. Rubio, Phys. Stat. Sol. B **243**, 2465 (2006); G. P. Zhang, D. A. Strubbe, S. G. Louie, and T. F. George, Phys. Rev. A **84**, 023837 (2011).
- [23] J. Yao *et al.*, Phys. Rev. Lett. **111**, 133001 (2013); B. Zhang, J. Yuan, and Z. Zhao, Phys. Rev. Lett. **111**, 163001 (2013).
- [24] S. N. Dixit and P. Lambropoulos, Phys. Rev. A **27**, 861 (1983); S. J. Bajic *et al.*, Phys. Rev.

- A **44**, 2102 (1991); S. T. Manson and A. F. Starace, *Rev. Mod. Phys.* **54**, 389 (1982).
- [25] I. V. Hertel, T. Laarmann, and C. P. Schulz, *Adv. At. Mol. Opt. Phys.* **50**, 219 (2005); E. E. B. Campbell, K. Hansen, K. Hoffmann, G. Korn, M. Tchapyguine, M. Wittmann, and I. V. Hertel, *Phys. Rev. Lett.* **84**, 2128 (2000).

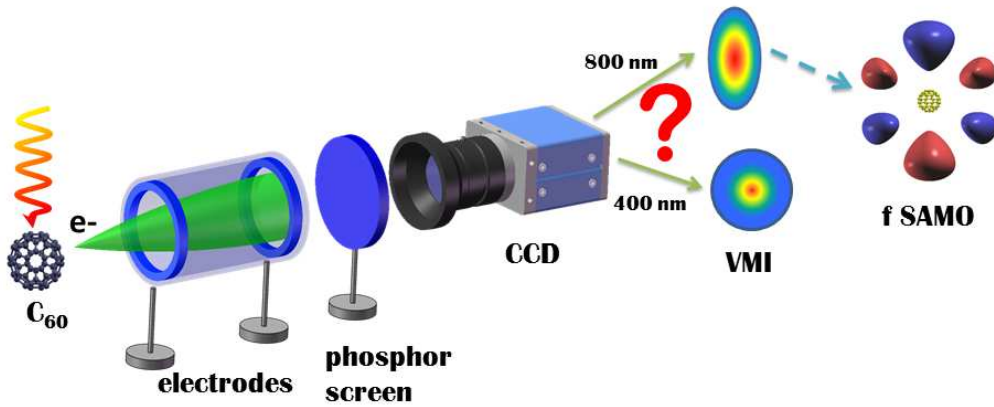


FIG. 1: Proposed experimental setup of velocity map imaging. Photoelectrons from C_{60} pass through electrode plates and form images on a phosphor screen, which are in turn captured by a CCD camera. Depending on whether an 800-nm or 400-nm laser is used, the image is anisotropic or isotropic. The diffuse origin of this image difference is attributed to the thermal photoelectron emission, but this can not explain the non-diffuse features seen in a recent experiment [19]. Far right: For convenience of viewing, we rotate the f superatomic molecular orbital (SAMO) by 90° .

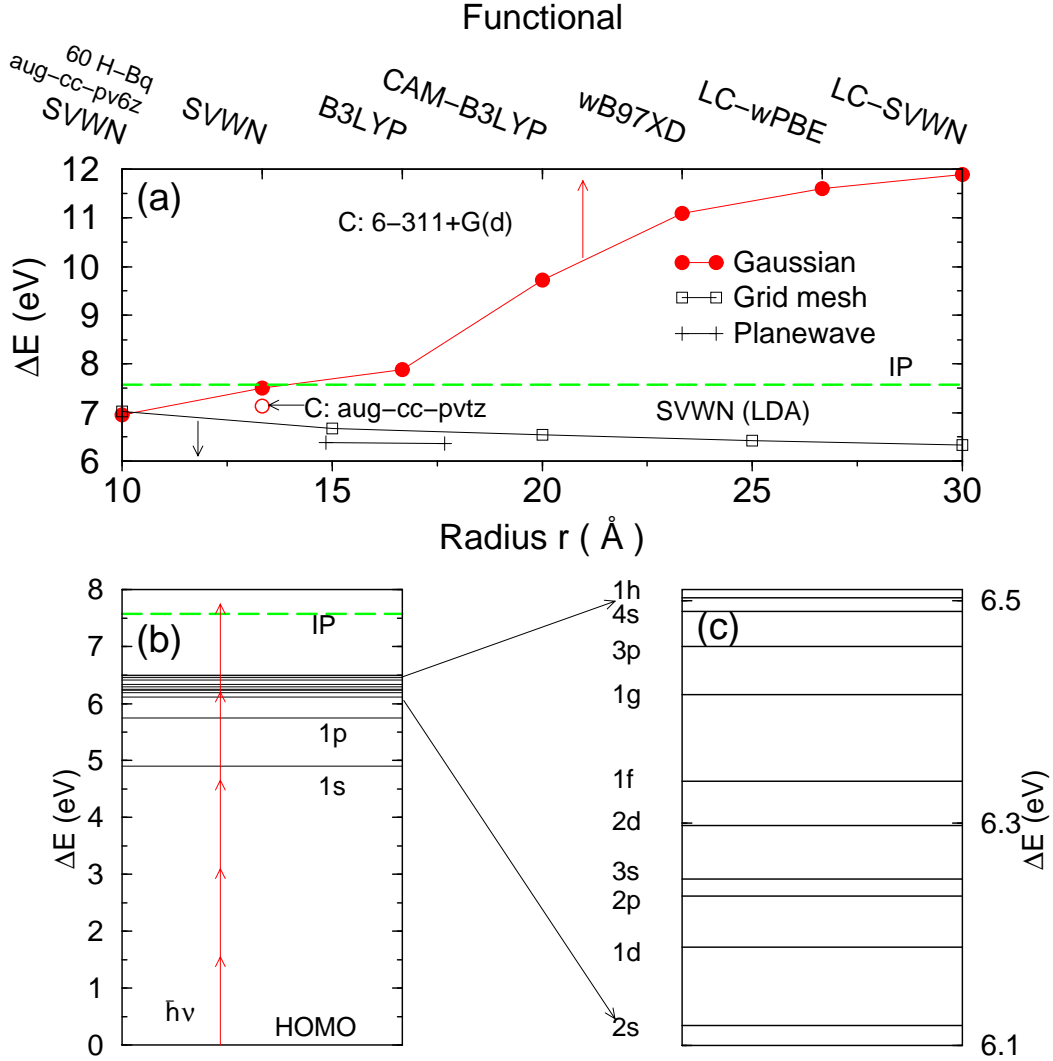


FIG. 2: (a) Energy gap between the $1f$ SAMO and HOMO computed with different functionals and basis functions (top axis) and as a function of sphere radius (bottom axis). The filled circles represent the results computed with Gaussian09, while the empty squares are those obtained with Octopus (the pseudopotential and on the real grid mesh). We expect that in the infinite sphere limit, the gap settles down at 6.2 eV. The VASP results (plus sign) are included for comparison, where the radius refers to the center-to-center distance of C_{60} . (b) Energy spectrum of SAMOs referenced to the HOMO energy. The ionization potential energy is at 7.58 eV (see the thick dashed green line at the top). (c) Zoomed-in SAMO energy spectrum. The $1f$ SAMO is between $2d$ and $1g$. The SAMOs form the doorway state for the ionization.

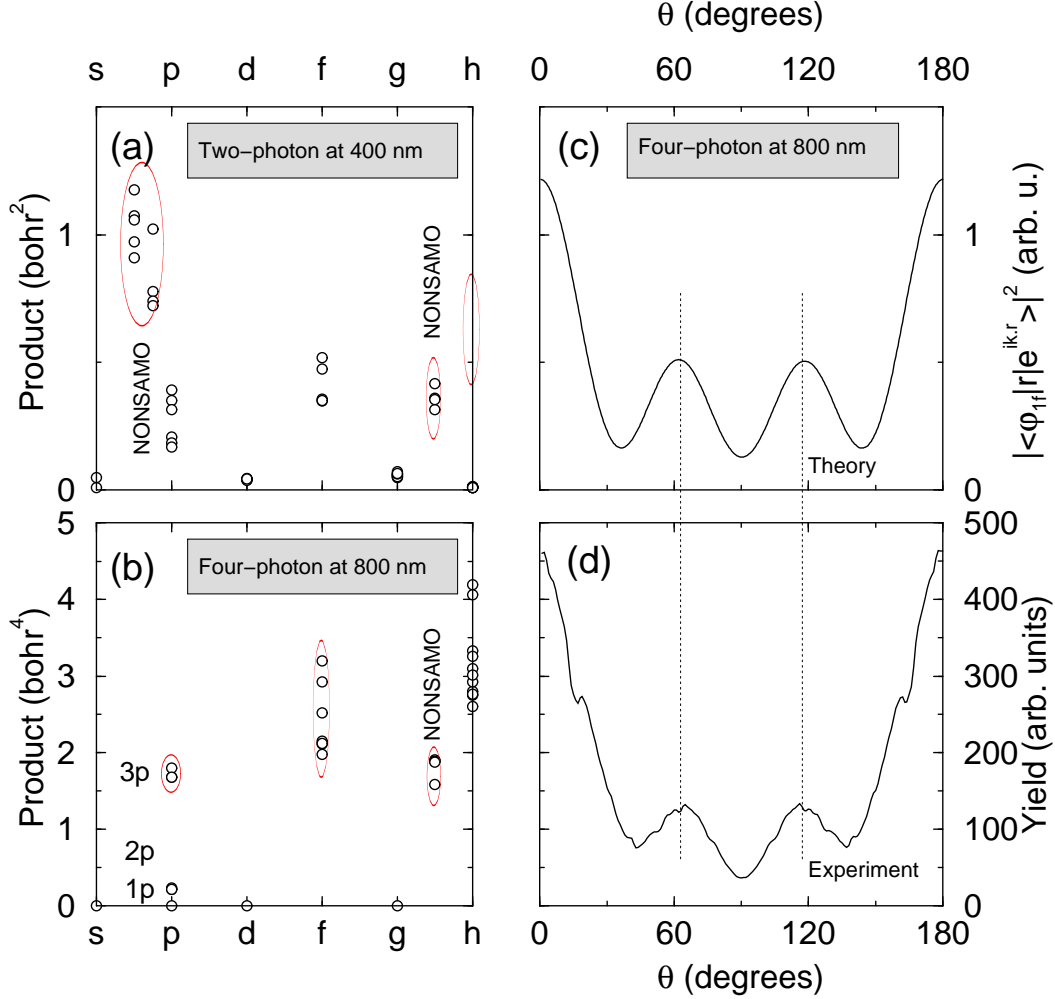


FIG. 3: (a) Product of two transition matrix elements for the two-photon process at the 400-nm wavelength. States that strongly contribute to the signal are highlighted with red ellipses. Although the nonSAMOs have a large transition matrix element, due to the off-resonance, their contribution is small. By contrast, 1s SAMO excitation is nearly resonant, so it dominates the photoelectron spectrum, consistent with the experimental findings. (b) Products of four transition matrix elements for the four-photon process excited at 800 nm. In contrast to (a), four SAMOs ($2p, 3p, 1f$ and $1h$) and one nonSAMO contribute strongly. Since only a subset of SAMOs are excited, this casts an anisotropic image. (c) Photoelectron angular distribution as a function of angle at 800 nm. Two humps are separated by 56.5° . (d) Experimental results from Ref. [19]. Excellent agreement with our theory is found.